Effect of biological polymers on mobility and run-out distance of cohesive and non-cohesive sediment gravity flows

Sobocinska, Alicja; Baas, Jaco

Marine Geology

DOI:
10.1016/j.margeo.2022.106904

Published: 01/10/2022

Peer reviewed version

Effect of biological polymers on mobility and run-out distance of cohesive and non-cohesive sediment gravity flows

Alicja Sobocinska [a] & Jaco H. Baas [a]

[a] School of Ocean Sciences, Bangor University, Askew Street, Menai Bridge, Isle of Anglesey, LL59 5AB, Wales, U.K.

ABSTRACT

Lock-exchange experiments were carried out to investigate the effect of biologically cohesive extracellular polymeric substances (EPS) on the mobility of sediment gravity flows laden with physically cohesive clay, non-cohesive coarse silt and non-cohesive fine sand. The results reveal significant differences in the head velocity, run-out distance and deposit shape of these flows related to differences in physical cohesion, particle size, and EPS content. These differences are captured in a three-way coupling model of turbulent forces, cohesive forces, and particle settling velocity. In general, biological cohesion reduces flow mobility, demonstrated most clearly by a progressive decrease in the run-out distance of the silt and clay flows, as the EPS concentration is increased. This reduction in flow mobility is caused by the dominance of cohesive forces over turbulent forces, which comprise turbulence attenuation and the bulk settling of a biologically cohesive gel in which EPS form a pervasive network of bonds between the sediment particles. However, sand-laden gravity flows were found to behave in a markedly different way, in that the head velocity and run-out distance first increase and then decrease, as the EPS concentration is increased. The increase in sand flow mobility is inferred to be caused by a reduction in the settling velocity of the sand particles, as the EPS cause an increase in flow viscosity at EPS concentrations that are sufficiently low to maintain turbulent flow. Once the EPS concentration is high enough for turbulence attenuation, the sand flows start to agree with the silt and clay flows in establishing a negative correlation between flow mobility and EPS concentration caused by gelling. The experimental data also uncovered that deposits formed by EPS-rich, turbulence-attenuated flows are shorter and thicker and have more abrupt terminations than deposits formed by EPS-free or EPS-poor turbulent flows. The larger thickness of these deposits is partly caused by the ability of EPS to retain water and form matrix-supported textures. Earlier work has shown that EPS is common in many sedimentary environments, including those where sediment transport takes place regularly by particulate density currents. Combined with the increasing rate at which man-made structures, such as pylons and communication cables, appear in these environments, we argue that there is a need to incorporate the results of this study in applied models that aim to mitigate damage to such structures by sediment gravity flows.

Key words: Sediment gravity flows; Physical experiments; EPS; cohesion; clay; silt; sand

1. Introduction

Sediment gravity flows (SGFs) comprise mixtures of water and sediment driven by excess density and gravity forces (Middleton and Hampton, 1973). Bottom-hugging SGFs originate from sediment-laden river flows that plunge after entering seas and lakes, i.e., hyperpycnal flows, and from slope failures caused by, for example, earthquakes, storm waves, slope oversteepening after rapid sedimentation, and fishing gear dragged across a loose substrate (Postma, 2011). SGFs are a global phenomenon, with the capacity of transporting large volumes of sediment, carbon, nutrients, and pollutants (e.g. microplastics) to the deep ocean (Postma, 2011; Baker et al., 2017; Heerema et al., 2019; Craig et al., 2020). These flows can cause serious damage to subaqueous communication cables and other deep-water engineering infrastructure (Inman et al., 1976; Talling et al., 2015), and they have been linked to the formation of tsunami (Johnson et al., 2017). Moreover, three-dimensionally stacked deposits of SGFs create submarine fans that are amongst the largest reservoirs of oil and gas on Earth (Reading and Richards, 1994; Heerema et al., 2019). Despite recent successes in studying SGFs in modern lakes and oceans (Talling et al., 2013; Zabala et al., 2017), and valuable understanding gained from traditional outcrop and core studies of SGF deposits, laboratory simulations remain a valued method for obtaining a physical understanding of the dynamics of SGFs and the style of their deposits (e.g. Baker et al., 2017; Craig et al., 2020). Laboratory experiments are unique in allowing the parameters that control the complex dynamics of SGFs to be studied in isolation. This includes SGFs that are cohesive because of the presence of physically active clay particles (Baker et al., 2017) and biologically active extracellular polymeric substances (EPS) (Craig et al., 2020). The effect of biological cohesion on the mobility of clay, silt, and sand flows is the principal target of the present study.

2. Background and rationale of study

2.1. Types of sediment gravity flow

SGFs have been classified using rheology and particle support mechanism (Middleton and Southard, 1984; Postma, 1986; Dasgupta, 2003; Haughton et al., 2009). In its simplest form, the rheological properties of a SGF can be characterized by yield strength, the resistance to deformation, and dynamic viscosity, the dependence of shear rate on applied shear stress (George and Qureshi, 2013; Widyatmoko, 2016). Turbidity currents are relatively dilute SGFs that exhibit Newtonian rheological behaviour (Middleton, 1993), i.e., without a yield strength and with a constant molecular viscosity (Chereskin and Price, 2001). Examples of denser SGFs with non-Newtonian behaviour are subaqueous debris flows, mud flows, and slides (Iverson, 1997). These flows may have a yield strength and a viscosity that decreases or increases as the shear stress is increased (Allen, 2009; Sumner et al., 2009; Manica, 2012). The main particle support mechanism in turbidity currents is turbulence (Middleton and Hampton, 1973; Heerema et al., 2019). Particles in debris flows, mud flows, and slides are supported mostly by matrix strength (Lowe, 1979; Dasgupta, 2003), provided by non-cohesive silt, physically cohesive clay (Baker et al., 2017) and biologically cohesive EPS (Craig et al., 2020). Cohesive forces tend to attenuate or fully suppress turbulent forces (Baker et al., 2017; Craig et al., 2020), often leading to a reduction in SGF mobility. Here, mobility is defined as the ability of SGFs to transport suspended load over a certain maximum distance, referred to as the run-out distance. Flow mobility is also governed by other processes, such as sediment erosion and deposition, mixing with ambient fluid, and particle settling velocity, as coarser particles are more likely to be deposited and less likely to be eroded from the sediment bed than finer particles, especially if these particles are non-cohesive.

The change from turbulent to turbulence-suppressed SGF depends on the flow velocity and the suspended sediment type and concentration, with high-velocity, low-viscosity flows more likely to be turbulent than low-velocity, high-viscosity flows. It is therefore not possible to define a single threshold sediment concentration for changes between turbidity current and mud or debris flow (Baker et al., 2017; Heerema et al., 2019). A range of transitional flows with both turbulent and laminar behaviour has been defined, including high-density turbidity currents (Middleton and Hampton, 1973; Lowe, 1982; Baker et al., 2017), lower and upper transitional plug flows (Baas et al., 2009, 2011), hybrid flows (Haughton et al., 2009), and top-transitional plug flows (Hermidas et al., 2018; Craig et al., 2020). Particularly relevant to this study are the high-density turbidity currents and top-transitional plug flows, which have a lower region of attenuated turbulence separated from a fully turbulent upper region where mixing with the ambient fluid takes place. Such flows are intermediate between fully turbulent, low-density turbidity currents and laminar mud or debris flows (called plug flows by Hermidas et al. [2018] and Craig et al. [2020]).

2.2. Sediment type and physical and biological cohesion

In the laboratory experiments with clay-laden and silt-laden SGFs of Baker et al. (2017), cohesion started to affect the flow mobility at a volumetric concentration of 10%. Above 10%, the head velocities of the flows started to diverge; the silt flows retained a higher velocity than the clay flows. This threshold concentration will vary with flow velocity, but this difference in flow mobility signifies a stronger network of particle bonds in the clay flows and therefore a stronger turbulence attenuation (e.g. Kuenen, 1965; Felix et al., 2005). Frictional forces started to reduce the mobility, and also the run-out distance, of the non-cohesive silt flows at concentrations that were at least three times greater than those of the clay flows (Baker et al., 2017; their figure 10).

More recent research by Craig et al. (2020) showed that biological cohesion can have a similar effect on the mobility of SGFs as physical cohesion, but at concentrations that are several orders of magnitude lower. Biological cohesion is caused by EPS secreted by microorganisms, such as diatoms and bacteria, mainly for protection, communication and interaction, carbon storage, nutrient entrapment, and aggregation (Wingender et al., 1999; Wolfaardt et al., 1999; Sandhya and Ali, 2015; Wang et al., 2015; Costa, 2018). These polymers form a gel-like, three-dimensional structure that stabilises the microbial aggregates via different physicochemical mechanisms, including dispersion forces, electrostatic interactions, and hydrogen bonds (Flemming et al., 2000). The microorganisms and their EPS are found in many depositional environments, from rivers and estuaries to hypersaline lakes and deep-sea hydrothermal vents (Decho and Gutierrez, 2017). EPS also act as a cohesive binder between the organisms and the surrounding sediment particles (Chenu, 1995; Wolfaardt et al., 1999), forming biofilms on the sediment surface that are resistant to erosion by overriding flows (Malarkey et al., 2015). Moreover, EPS induce more pervasive cohesion in muddy and sandy substrates below biofilms (e.g. Malarkey et al., 2015; Hope et al., 2020) and assist in flocculation and gelling of clay in suspension flows (Flemming and Wingender, 2010; Gerbersdorf and Wieprecht, 2014). Craig et al. (2020) found that the mobility of SGFs carrying 15%, 22% and 23% kaolinite clay was reduced significantly by adding between 0.052% and 0.265% by weight of EPS, matching concentrations measured by Craig et al. (2020) in surficial deep-water sediment offshore New Zealand.

2.3. Research aims

The present study aims: (a) to determine the effect of non-cohesive silt and sand on the mobility of SGFs with and without EPS; (b) to compare the effect of EPS on flow mobility between physically cohesive and non-cohesive SGFs. Craig et al. (2020) used mixtures of clay and EPS, but SGFs also carry non-cohesive silt and sand (Kuenen, 1951; Britter and Simpson, 1978; Parker et al., 1987; Middleton and Neal, 1989; Baas et al., 2005). Like clay-laden SGFs, silt and sand flows may contain EPS supplied from the source area or eroded from the basin floor during transport. We hypothesise that EPS change the flow properties from Newtonian turbidity currents to non-Newtonian transitional flows and mud or debris flows with attenuated turbulence, which in turn reduces the flow velocity and run-out distance, and modifies the properties of their deposits, as for the mixed clay–EPS flows of Craig et al. (2020). Testing this hypothesis is essential for mitigating damage to subaqueous engineering infrastructure, forecasting the dispersal of nutrients and pollutants in the deep sea, and predicting the three-dimensional architecture of submarine fans.

3. Methods

Eleven laboratory experiments were conducted using a lock-exchange tank, 5 m long, 0.2 m wide and 0.5 m deep, in the Hydrodynamic Laboratory, School of Ocean Sciences, Bangor University (Fig. 1). The 0.31-m long reservoir behind the lock gate was filled with 0.3 m of a sediment–water or sediment–EPS–water mixture, while the channel downstream of the lock gate was filled with water only to the same depth. All experiments used natural seawater (density, ρ = 1027 kg m^{-3}; salinity, s = 35 PSU) sourced from the Menai Strait, a tidal strait next to the Hydrodynamic Laboratory. Three different sediment types were used: cohesive kaolin clay (median size, D_{50} = 0.0091 mm); non-cohesive, very well-sorted, silt-sized, spherical glass beads (D_{50} = 0.050 mm); and non-cohesive, very well-sorted, sand-sized glass beads (D_{50} = 0.213 mm). All experiments used a volumetric sediment concentration of 15% and weight concentrations of EPS of 0%, 0.15%, and 0.3%. The sand experiments used additional EPS concentrations of 0.05% and 0.2%. Xanthan gum was used to represent natural EPS (cf., Malarkey et al., 2015; Craig et al., 2020). These sediment and xanthan gum concentrations were informed by the SGF experiments of Baker et al. (2017) and Craig et al. (2020).

Each starting suspension in the reservoir was prepared in the same way to account for any time-dependent behaviour, following procedures described by Baker et al. (2017) and Craig et al. (2020). First, the xanthan gum and sediment were mixed in dry form in a concrete mixer for 10 minutes. The seawater was then added to the dry material and mixed for another 10 minutes. Subsequently, the wet slurry was decanted into a large bucket and mixed for another 3 minutes with a handheld mixer to break up any remaining clumps of sediment. The slurry was then left to rest for 60 minutes, before being mixed a third time for 3 minutes (except for the silt–water mixture which required 6 minutes of mixing). Thereafter, a 180-ml subsample was taken from the slurry (except for 0.2% EPS sand) for subsequent particle settling velocity analysis and the slurry was added to the reservoir in the lock-exchange tank and mixed for 30 seconds with the handheld mixer, before lifting the lock gate and thus generating a bottom-hugging SGF. The moving head of each SGF was recorded using a high-definition video camera, with the aim to document changes in head shape, internal flow structure, and head velocity, following procedures described by Baker et al. (2017). Deposit thicknesses were recorded along the sidewall of the tank for the SGFs that halted before reaching the end of the tank. Replicates of three sand experiments showed that head velocities and run-out distances of the SGFs were reproducible (Table 1).

The 180-ml subsamples were used to determine particle settling velocities of the 15% pure sediment and mixed EPS–sediment suspensions. This involved timing the falling interface between clear water and the settling suspension in the sampling container, after fully homogenising the starting suspension, following the procedure described by Baas et al. (2022, their figure 1).

Head velocities of the SGFs were calculated from the video footage at a spatial resolution of 0.1 m along the tank using Microsoft Movie Maker. With the exception of the clay flows laden with 0.3% EPS, each SGF could be subdivided into a period of constant head velocity followed by a period of waning head velocity. The period of constant head velocity was characterised by the mean pre-deceleration head velocity between 23% and 64% of either the run-out distance (red segment of the blue curve in Fig. 2) or 4.6 m for flows that reflected off the end of the tank (Fig. 2). For most SGFs that stopped before reaching the end of the tank — referred to as the main flow below — a dilute cloud bypassed the deposit of the main flow. This cloud, referred to as the bypassing flow below, continued to move down the tank at a slower rate than the main flow. The velocity of these bypassing flows was measured using the same method as for the main flow (orange curve in Fig. 2).

4. Results

4.1. Settling velocity experiments

4.1.1. EPS-free sediment

The EPS-free 15% kaolin clay suspension had a settling velocity at 0.0025 mm s^{-1} (Fig. 3). This was two orders of magnitude lower than the settling velocity of the EPS-free 15% coarse silt suspension. As expected, the EPS-free 15% fine sand suspension had the highest settling velocity of 4.7 mm s^{-1} (Fig. 3).

4.1.2. EPS–sediment mixtures

All EPS-laden suspensions had a lower settling velocity than the equivalent EPS-free suspensions, and the settling velocity decreased, as the EPS concentration was increased, for all sediment types (Fig. 3). This decrease stretched over five orders of magnitude for the non-cohesive silt and sand suspensions, but the decrease was confined to a factor of only 4.5 for the cohesive clay suspensions between 0% and 0.30% EPS. Moreover, Fig. 3 shows that the greatest decrease in settling velocity for the silt suspensions was between 0% and 0.15% EPS, whereas the decrease in the settling velocity for the sand suspensions was relatively small between 0% and 0.05% EPS. At 0.30% EPS, the settling velocities were within one order of magnitude for the three sediment types (Fig. 3). Hence, the particle settling was less dependent on sediment type and size at 0.30% EPS than at lower EPS concentrations.

4.2. Visual observations and flow type classification

Five out of the eleven experimental runs conducted, i.e., all EPS-free flows and flows Sa-0.05 and Sa-0.15 (Table 1), were characterised by fully turbulent behaviour. The head of these flows had a pointed, semi-elliptical shape with a prominent nose in a vertical section parallel to the flow direction (Fig. 4A; Table 1). These flow properties match the low-density turbidity currents of Baker et al. (2017; their table 3) and the turbidity currents s.s. of Craig et al. (2020; their table 2).

Flows Cl-0.15, Si-0.3 and Sa-0.3 consisted of a dense lower layer, in which turbulence attenuation was clearly visible, and a more dilute, lighter-coloured and fully turbulent, upper layer, characterised by mixing with the ambient water (Fig. 4B; Table 1). In combination with hydroplaning at the base of the head of these flows (Fig. 4B), the presence of linear coherent fluid entrainment structures (*sensu* Baker et al., 2017; Figs. 4C, D) and a more rounded flow front than the low-density turbidity currents, these flows resemble the high-density turbidity currents of Baker et al. (2017; their table 3) and the top-transitional plug flows of Hermidas et al. (2018) and Craig et al. (2020; their table 2). High-density turbidity currents Cl-0.15, Si-0.3 and Sa-0.3 also included a dilute turbulent flow released from the upper part of the main flow after it stopped moving (Figs. 4E, F). These bypassing flows moved slowly down the tank.

Flows Si-0.15 and Sa-0.2 (Table 1) started as fully turbulent low-density turbidity current but they changed to stratified high-density turbidity current in the final phase of movement by vertical settling of sediment particles into the lower part of the flow. Flow Sa-0.2 exhibited coherent fluid entrainment structures, but fewer than in the high-density turbidity currents.

Finally, flow Cl-0.3 slid out of the reservoir as a coherent mass of sediment; it was devoid of any internal turbulence (Figs. 4G, H; Table 1). This viscous flow, which showed little mixing at the top and lacked hydroplaning, is classified as a slide (Baker et al., 2017 [their table 3]; Craig et al., 2020 [their table 2]). Immediately after the slide had stopped moving, a dilute turbidity current formed at the top of the slide. This current bypassed the front of the slide and then moved slowly towards the downstream end of the tank.

The flow types defined in this paper are plotted as a function of EPS concentration and sediment type in Fig. 5. This flow-type phase diagram reveals that the boundaries between low-density turbidity currents, transitional low-density to high-density turbidity currents, high-density turbidity currents, and slides move to higher EPS concentrations, as the sediment type changes from clay via coarse silt to fine sand. Fig. 5 also shows a stability field for mud flows, in the case of suspended clay, or debris flows, in the case of suspended silt or sand (*sensu* Baker et al., 2017), equivalent to the plug flows of Hermidas et al. (2018) and Craig et al. (2020; their table 2). These flow types were not observed in the present experiments, but they are expected in clay flows that contain between c. 0.2% and 0.25% EPS.

4.3. Flow velocity and run-out distance

4.3.1. EPS-free control experiments

The EPS-free clay and silt flows behaved in a similar manner hydrodynamically. Both flows had a mean pre-deceleration head velocity of 0.35 m s^{-1} down to a distance, *x*, of 3 m along the tank (Figs. 6A, 7). The head velocity of these flows then gradually decreased to c. 0.2 m s^{-1}, before the flows reflected off the end of the tank (Figs. 6A,B, 8).

In contrast, the EPS-free sand flow decelerated earlier than flows Cl-0 and Si-0. After maintaining a mean pre-deceleration head velocity of 0.34 m s^{-1} for 1.2 m, flow Sa-0 waned quickly, reaching a run-out distance of 2.5 m (Figs. 6C, 7, 8). A weak bypassing flow formed after the main flow had stopped, but it lost forward momentum quickly and ran out at x = 3 m (Fig. 6C).

4.3.2. Mixed sediment–EPS experiments

The head velocity profiles and run-out distances of the EPS-laden flows varied with sediment type and EPS concentration (Figs. 6–8). Except for slide Cl-0.3, which started to decelerate immediately after leaving the reservoir, all flows were similar to the EPS-free control flows in that the head velocity was constant for a certain distance along the tank, before the flow started to decelerate exponentially. The differences in mean pre-deceleration head velocity were small, ranging from 0.32 m s^{-1} to 0.37 m s^{-1} across all sediment types and EPS concentrations, again excluding slide Cl-0.3 (Fig. 7; Table 1). Yet, Fig. 7 reveals that the mean pre-deceleration head velocity in the mixed clay–EPS and silt–EPS flows decreased slightly, as the EPS concentration was increased and the flows changed from low-density to high-density turbidity current in the silt runs and from low-density turbidity current to slide in the clay runs. In contrast, the mean pre-deceleration head velocity in the mixed sand–EPS flows increased from 0% to 0.05% EPS and decreased from 0.15% to 0.30% EPS (Fig. 7). These trends are mimicked by changes in the location at which the flows started to decelerate, and, particularly, by changes in the run-out distance of the flows (cf. Figs. 7, 8). The run-out distance of the mixed clay–EPS and silt–EPS flows decreased, as the EPS concentration was increased, and the run-out distance in the mixed sand–EPS flows reached a maximum value of 4.4 m around 0.15% EPS (Fig. 8). Fig. 8 also shows that the run-out distance of the clay flows decreased more rapidly with increasing EPS concentration than the run-out distance of the silt flows and that the run-out distances of flows Si-0.20 and Si-0.30 merge with those of flows Sa-0.20 and Sa-0.30 (Fig. 8). This merging of run-out distances thus appears to be confined to the turbulence-attenuated turbidity currents carrying non-cohesive coarse silt and fine sand.

4.4. Deposit properties

The shape and thickness distribution of the deposits formed by the experimental flows varied with sediment type and EPS concentration, and therefore with flow type. The deposit of slide Cl-0.30 was short and thick; it dipped steeply and almost uniformly from the point of entry into the tank (Fig. 9A). The deposits of the low-density turbidity currents and the transitional low-density to high-density turbidity currents tended to be wedge-shaped, with a gradual termination near the location of run-out (e.g. flows Sa-0 and Sa-0.20; Fig 9B). The high-density turbidity current deposits had a more abrupt termination, which is most apparent in the deposit of flow Cl-0.15 (Fig. 9A). The EPS-free and low-EPS silt and sand flows formed firm deposits, whereas adding large amounts of EPS to these flows resulted in soft, water-rich and gel-like beds. Such EPS-rich beds were significantly thicker than the EPS-free and EPS-poor beds (e.g. Fig. 9B).

5. Discussion

5.1. Controlling factors on the mobility of the biologically cohesive flows

The amount of EPS added to the flows was two orders of magnitude lower than the sediment concentration, i.e., 0–0.3% EPS versus 15% sediment. The density difference with the ambient water, which drives the mobility of sediment gravity flows (Middleton and Hampton, 1973; Kneller and Buckee, 2000), was therefore nearly constant and unable to explain the observed variations in flow mobility and run-out distance. Other factors that controlled the flow mobility and run-out distance in the experiments were: (1) drag-induced turbulent forces; (2) cohesive forces of physical and biological origin, caused by kaolin clay and EPS, respectively; (3) particle settling velocity; and (4) hydroplaning (e.g. Middleton and Hampton, 1973; Lowe, 1982; Mohrig *et al*., 1998; Baker *et al*., 2017; Craig et al., 2020). Upward-directed turbulent forces tend to promote flow mobility by keeping particles in suspension and therefore maintaining the density difference with the ambient water (Middleton and Hampton, 1973). However, turbulent forces are counteracted by cohesive forces and particle settling, which both tend to hinder flow mobility and promote deposition. The settling velocity of single particles increases with increasing particle size, but it decreases with increasing particle concentration, because of the hindered settling effect (e.g. Richardson and Zaki, 1954; Baas et al., 2022). However, the effect of hindered settling on flow mobility is expected to have been small in the experiments, because all flows carried the same volumetric concentration of sediment particles. Hydroplaning reduces the drag at the base of dense SGFs and it therefore promotes flow mobility and run-out distance (Mohrig et al., 1998). Below, the combined effect of turbulent forces, cohesive forces, particle settling velocity, and hydroplaning is used to explain the differences in mobility between the experimental flows.

5.2. Comparison of flow mobility: EPS-free control flows

All the EPS-free SGFs behaved as fully turbulent, low-density turbidity currents (*sensu* Baker et al. 2017). However, the mean pre-deceleration head velocity of flow Sa-0 was slightly lower than that of flow Cl-0 and Si-0 (0.34 m s^{-1} and 0.35 m s^{-1}, respectively; Table 1) and flow Sa-0 started to decelerate c. 1.5 m earlier than the finer-grained flows (Fig. 6). These differences are inferred to reflect the higher single particle settling velocity of the fine sand (Fig. 3), which worked against the upward-directed particle support by turbulence and caused the flow Sa-0 to have a significantly shorter run-out distance than flows Cl-0 and Si-0 (Fig. 8). The role of physical cohesion in flow Cl-0 was small, considering that the non-cohesive silt flow and the cohesive clay flow had almost identical head velocity profiles (Fig. 6). This agrees with Baker et al. (2017), who found that their 15% fine silt and kaolin flows had similar mean head velocities.

5.3. Comparison of flow mobility: Biologically cohesive flows

Our hypothesis that biologically cohesive EPS reduce the flow mobility, i.e., the run-out distance (Fig. 8), is supported for the silt and clay flows. This reduction is also expressed by a lower mean pre-decelerating head velocity (Fig. 7). The biologically cohesive forces induced by the EPS attenuated the turbulence and changed the low-density turbidity currents to high-density turbidity currents (*sensu* Lowe, 1982), and eventually to slides (Mohrig and Marr, 2003) at the maximum EPS concentration in the clay flows (Table 1). These changes in flow type were accompanied by a reduction in the run-out distance through a change in the settling behaviour from single particle settling and hindered settling to bulk, ‘en-masse’, settling of gel-like substances, in which the EPS form a volume-filling network of bonds between the clay or silt particles (Craig et al., 2020). Flow transformation along the tank from low-density to high-density turbidity current, i.e., from fully turbulent flow to top transitional plug flow (Hermidas et al., 2018; Craig et al., 2020), signifies a downflow shift in the force balance from dominantly turbulent to dominantly cohesive during the deceleration phase, resulting in bulk settling.

In contrast to the similarities in the mobility of the pure silt and clay flows, described above, the clay–EPS flows started to decelerate earlier and had shorter run-out distances than the silt–EPS flows (Fig. 6). These differences in the influence of biological cohesion may have two possible causes. Firstly, as for clay concentration, EPS concentration has an exponential relationship with flow viscosity and yield strength (e.g. Wan, 1982). Therefore, adding EPS to an already weakly cohesive clay flow may lead to a larger reduction in flow mobility than adding the same amount of EPS to a non-cohesive silt flow, even if this difference in physical cohesion is not reflected in a significant difference in the head velocity profile between these EPS-free flows (Figs. 6A, B). This interpretation assumes that sediment particles and EPS act independently in changing the cohesion of the flows. This assumption is not necessarily valid, because different types of sediment and EPS may interact in yet unknown ways in gravity flows. Further work is needed to explore such interactive processes. Secondly, the total particle surface area in clay flows is larger than in silt flows, because of the larger number of particles for a given concentration, which might increase the ease with which to establish particle bonds by EPS in the clay flows and thus a stronger network of particle bonds (Craig et al., 2020).

The sand flows are more complex than our hypothesis advocates, because the run-out distance, in particular, in the EPS-free sand flow was shorter than in the sand flows with low EPS concentrations. This can be explained by a three-way coupling between turbulence, cohesion, and settling velocity. EPS increase the viscosity of the water (Craig et al., 2020), which decreases the settling velocity of sand particles and allows the sand to be kept in suspension for longer. In turn, this promotes the run-out distance. However, this is valid only for flows in which the EPS concentration is low, so that the flow remains turbulent. At high EPS concentrations, the sand flow becomes transitional or laminar and behaves in a similar way to the silt and clay flows, despite the even lower settling velocity of sand in these EPS-rich flows. In other words, particle size is less important in controlling flow mobility in EPS-rich high-density turbidity currents, mud or debris flows, and slides. This is supported by the results of the settling experiments, which show that the clay, silt, and sand flows had more similar settling velocities at 0.3% EPS than at lower EPS concentrations (Fig. 3) and that the run-out distances of the silt and sand flows merged at 0.2% and 0.3% EPS (Fig. 8). As in the silt-laden and clay-laden high-density turbidity currents and slides, bulk settling of a cohesive gel with pervasively bonded sand particles explains why the EPS-rich sand-laden high-density turbidity currents became less mobile and had a shorter run-out distance (Fig. 8).

Hydroplaning was confined to high-density turbidity currents in the experiments. This phenomenon occurs when the weight per unit area of material, here sediment and EPS, in the head of a flow is exceeded by the dynamic pressure generated by the fluid just below the head (Mohrig et al., 1998; Mohrig et al., 1999). Moreover, it is essential to prevent mixing of the overridden water with the flow above, thus the permeability of the base of the flow has to be sufficiently low (Talling, 2013). This was achieved fully in all the high-density turbidity currents, because of the high physical and biological cohesive strength of these flows. Hydroplaning, however, did not occur in the low-density turbidity currents, because the turbulence caused immediate mixing of water getting underneath the head of these flows (cf., Baker et al., 2017). The base of the mixed clay–EPS slide probably was sufficiently impermeable, but it did not allow hydroplaning either, because its low flow velocity prevented ambient water from being forced underneath the head of the slide. Hydroplaning in the high-density turbidity currents should have reduced the drag with the bed, but the shorter run-out distance of these flows compared to the low-density turbidity currents suggest that the effect of increased cohesion outweighed that of hydroplaning.

5.4. Comparison of deposits

The deposits of all the low-density turbidity currents that stopped before reaching the end of the lock-exchange tank were thin and wedge-shaped (Fig. 9), which is typical for turbulent flows that comprise progressive single-particle settling and hindered settling (Baker et al., 2017). This includes the low-EPS sand flows that were more mobile than the EPS-free sand flow, thus confirming that the EPS concentration in these flows was sufficiently low to prevent the flow from turning into a cohesive gel. The high-density turbidity currents and the slide, on the other hand, produced relatively thick deposits with a more abrupt termination, typical for bulk settling of cohesive gels (Baker et al., 2017; Fig. 9). The unusually large thickness of the EPS-rich deposits (Fig. 9) is testament to the ability of the EPS to retain water in the cohesive gel and prevent the deposit from attaining a grain-supported texture (Craig et al., 2020). As in physically cohesive clay beds (Mehta, 2013), such fluid-mud like deposits may take many months to consolidate to firm deposits.

5.5. Implications for natural biologically cohesive flows and deposits

The present laboratory experiments show that EPS have a significant influence on the mobility and run-out distance of cohesive and non-cohesive SGFs and on the shape of their deposits. As such, our experiments extend the SGF experiments with mixed clay–EPS of Craig *et al*. (2020) to mixed silt–EPS and sand–EPS SGFs, and provide evidence that particle size, in addition to turbulence and cohesion, needs to be considered in predicting the behaviour of biologically cohesive SGFs (Fig. 10). The inferred three-way coupling between particle settling velocity, turbulent forces and cohesive forces dictates that EPS can increase the flow mobility, if EPS increase the flow viscosity whilst keeping the flow turbulent, and decrease the flow mobility, if EPS attenuate the turbulence and change the flow to a cohesive gel (Fig. 10). Within the parameter space of the experiments, mobility enhancement is characteristic of sandy low-density turbidity currents, and mobility reduction is typical of high-density currents, slides, and probably also mud flows and debris flows (Fig. 10).

These fundamental physical outcomes should also be relevant to natural flows. However, scaling of the experimental flows to natural prototypes is not possible at present, because standard scaling methods do not allow for the inclusion of physical and biological cohesion in SGFs. Moreover, natural SGFs are more complex than the experimental flows simulated here; for example, single-particle size flows moving across a smooth, horizontal bed are an exception, rather than rule, in nature. In regard to flow velocity, the experimental SGFs are suitable analogues for hyperpycnal flows at river mouths and weak, single-surge, submarine SGFs triggered by earthquakes (Talling et al., 2013), sustained SGFs with a frontal high-density basal layer (Zabala et al., 2017), and natural SGFs that have decelerated to a similar velocity as in the experiments. It should also be mentioned that the experiments used a single type of clay and EPS. The rheological properties of clay and EPS vary with chemical composition. For example, kaolin clay has a lower cation exchange capacity, a key parameter for describing cohesive properties (Yong et al., 2012), than illite and montmorillonite, which are also common in prototype flows and deposits. Under given hydrodynamic conditions and clay concentration, SGFs laden with illite or montmorillonite should therefore lose mobility at lower EPS concentrations than kaolinite-laden flows, and thus be more prone to change from low-density turbidity current to high-density turbidity current, mud flows and slide.

The maximum EPS concentration of 0.3% used in the experiments was informed by the maximum EPS concentration found in the seabed offshore New Zealand (Craig et al., 2020). Unless higher EPS concentrations can be established elsewhere, ≤ 0.3% EPS contained in faster flows should have a smaller effect on flow mobility, since turbulent forces are positively correlated with flow velocity. Some support is provided by the experiments of Craig et al. (2020), since their SGFs laden with 15% kaolin clay were faster than in the present study (0.42 m s^{-1} versus 0.35 m s^{-1}), and the reduction in run-out distance for EPS concentrations up to 0.265% was less than in the present experiments. The exception may be the increased mobility of sandy SGFs with low concentrations of EPS, as the behaviour of these flows is more dependent on the particle settling velocity than on turbulence attenuation.

The shape of deposits of natural SGFs are expected to mimic that of the experimental SGFs. EPS generally cause SGF deposits to become shorter and thicker, except for deposits formed by high-mobility SGF laden with sand and low concentrations of EPS. These differences in shape can be expressed at first order by a deposit steepness parameter, *S*:

$$S = arctan\left(\frac{h_{max}}{X_R}\right), \tag{1}$$

where h_{max} is the maximum deposit thickness, X_R is the run-out distance, and *S* is given in degrees. The deposit steepness parameter is plotted against EPS concentration in Fig. 11 for the deposits of all flows that stopped before reaching the end of the tank. Short and thick deposits are expressed by relatively high *S* values, whereas long and thin deposits have low *S* values. Fig. 11 shows that EPS-laden clay flows form steeper deposits than sand and silt flows, because of their lower mobility induced by combined physical and biological cohesion. Natural deposits of EPS-free sand flows are expected to have higher *S* values than deposits of low-EPS sand flows, here for 0.05–0.2% EPS, because of their low viscosity and high sand settling velocity. At high EPS concentrations, here for 0.2% and 0.3% EPS, the deposit steepness increases with increasing EPS concentration for SGFs laden with clay or sand (Fig. 11), and presumably also for silt-laden flows, because of reduced flow mobility caused by greater biological cohesion. The steepness of deposits of low-EPS sand flows, here for 0.05–0.2% EPS, is proportional to EPS concentration on a logarithmic scale (Fig. 11). Despite the observed increase in mobility of these flows, which would cause the deposits to become longer and thinner and thus *S* to become lower, anomalously high increases in deposit thickness lead the increase in the steepness parameter, because of the above-mentioned development of soft, water-rich and gel-like beds. However, such beds may be unstable and bed consolidation by water expulsion may lead to a rapid decrease in deposit thickness, and therefore deposit steepness, under natural conditions. For natural hydrodynamic conditions comparable to those simulated in the experiments, the *S* values of deposits formed by high-EPS sand-laden and silt-laden SGFs, here for 0.3% EPS, are expected to be similar (Fig.

11). This supports the above interpretation that the size of non-cohesive particles becomes less important as the EPS concentration increases.

Because SGFs in nature can have run-out distances of hundreds to even thousands of kilometres, the results of this study should be included in the mitigation of possible damage to subaqueous infrastructure that is in the path of SGFs. If the sediment in the source area of these SGFs, as well as the sediment eroded from the bed during transport, is dominated by silt or clay, the presence of EPS in these flows can be expected to reduce the risk of damage to, for example, subaqueous pylons and communication cables. Although turbulent sand-rich SGFs generally are less mobile than turbulent silt-rich and clay-rich SGFs, and therefore, less likely to reach subaqueous infrastructure from the same source area, the enhanced mobility of sand flows carrying small amount of EPS may lead to a false sense of security, because such flows may travel further than expected.

6. Conclusions

The laboratory experiments presented in this paper reveal that the mobility of biologically cohesive sediment gravity flows and the shape of their deposits depend on the type and size of suspended particles, i.e., physically cohesive clay versus non-cohesive silt and sand, and the concentration of extracellular polymeric substances. Upon the addition of EPS at concentrations typical of deep-marine environments, the induced biological cohesion causes fine-grained EPS-free flows to become turbulence-attenuated, leading to a reduction in flow mobility. This reduction in mobility is reflected in the progressive shortening of the run-out distance of the flows, as the EPS concentration is increased. In contrast to clay and silt flows, the mobility of sand flows is affected not only by the balance between turbulent and cohesive forces, but also by the high settling velocity of the sand particles. The high settling velocity causes a low flow mobility under EPS-free conditions, reflected in a short run-out distance. However, the presence of EPS in sand flows induces a considerable increase in run-out distance by increasing the flow viscosity, provided that the EPS concentration is sufficiently low to prevent turbulence attenuation in these flows. Above a certain threshold EPS concentration, sand flows become less mobile and behave in a similar way to silt flows and clay flows, because the formation of a biologically cohesive gel renders the settling velocity of subordinate importance. Since EPS has been shown to be pervasive in depositional environments where sediment gravity flows are expected to occur and where engineering infrastructure is being constructed at an increasing rate, these results need to be incorporated in models that aim to mitigate damage to such infrastructure.

All experimental data are available on FigShare via DOI 10.6084/m9.figshare.19960151 and URL https://figshare.com/articles/dataset/Data_tables_for_Figs_3_6_9_docx/19960151.

Acknowledgements

The hydrodynamic data presented in this paper were acquired as part of an MSci (Integrated Master) project by the leading author at the School of Ocean Sciences at Bangor University. The authors are grateful for the constructive comments of journal reviewers Sanem Acikalin, Rafael Manica, and Chris Stevenson, as well as editor-in-chief Michele Rebesco, which greatly improved the original manuscript. This project was partly funded by a research grant from Equinor, Norway.

References

Allen, P.A., 2009. Earth Surface Processes. John Wiley & Sons, Hoboken, New Jersey. 432 p.

Baas, J.H., 2005. Sediment gravity flows: Recent advances in process and field analysis—Introduction. Sedimentary Geology, 179, 1–3. https://doi.org/10.1016/j.sedgeo.2005.05.003

Baas, J.H., Baker, M.L., Buffon, P., Strachan, L.J., Bostock, H.C., Hodgson, D., Eggenhuisen, J.T. and Spychala, Y.T., 2022. Blood, lead and spheres: A hindered settling equation for sedimentologists based on metadata analysis. The Depositional Record, 8, 603–615. https://doi.org/10.1002/dep2.176

Baas, J.H., Best, J.L. and Peakall, J., 2011. Depositional processes, bedform development and hybrid bed formation in rapidly decelerated cohesive (mud–sand) sediment flows. Sedimentology, 58, 1953–1987. https://doi.org/10.1111/j.1365-3091.2011.01247.x

Baas, J.H., Best, J.L., Peakall, J., and Wang, M., 2009. A phase diagram for turbulent, transitional, and laminar clay suspension flows. Journal of Sedimentary Research, 79, 162–183. https://doi.org/10.2110/jsr.2009.025

Baker, M.L., Baas, J.H., Malarkey, J., Jacinto, R.S., Craig, M.J., Kane, I.A. and Barker, S., 2017. The effect of clay type on the properties of cohesive sediment gravity flows and their deposits. Journal of Sedimentary Research, 87, 1176–1195. https://doi.org/10.2110/jsr.2017.63

Britter, R.E. and Simpson, J.E., 1978. Experiments on the dynamics of a gravity current head. Journal of Fluid Mechanics, 88, 223–240. https://www.cambridge.org/core/journals/journal-of-fluid-mechanics/article/abs/experiments-on-the-dynamics-of-a-gravity-current-head/C2B7F72B6AA2834A3DCC5DA3FAFA13E8

Chenu, C., 1995. Extracellular polysaccharides: An interface between microorganisms and soil constituents, in Huang, P.M., Berthelin, J., Bollag, J. M., Mcgill, W.B. and Page, A.L. (Eds.), Environmental Impact of Soil Component Interactions. Natural and Anthropogenic Organics, Boca Raton, FL: CRC Lewis Publishers, pp. 217–234.

Chereskin, T.K. and Price, J.F., 2001. Ekman transport and pumping, in: Steele, J.H., Thorpe, S.A. and Turekian, K.K. (Eds.), Ocean Currents: A derivative of the encyclopedia of Ocean Sciences. Academic Press, pp. 809–815.

Costa, O.Y.A., Raaijmakers, J.M. and Kuramae, E.E., 2018. Microbial extracellular polymeric substances: Ecological function and impact on soil aggregation. Frontiers in Microbiology. https://doi.org/10.3389/fmicb.2018.01636

Craig, M.J., Baas, J.H., Amos, K.J., Strachan, L.J., Manning, A.J., Paterson, D.M., Hope, J.A., Nodder, S.D. and Baker, M.L., 2020. Biomediation of submarine sediment gravity flow dynamics. Geology, 48, 72–76. https://doi.org/10.1130/G46837.1

Dasgupta, P., 2003. Sediment gravity flow—The conceptual problems. Earth-Science Reviews, 62, 265–281. https://doi.org/10.1016/S0012-8252(02)00160-5

Decho, A.W., and Gutierrez, T., 2017. Microbial extracellular polymeric substances (EPSs) in ocean systems. Frontiers in Microbiology. https://doi.org/10.3389/fmicb.2017.00922

Felix, M., Sturton, S. and Peakall, J., 2005. Combined measurements of velocity and concentration in experimental turbidity currents. Sedimentary Geology, 179, 31–47. https://doi.org/10.1016/j.sedgeo.2005.04.008

Flemming, H.-C. and Wingender, J., 2010. The biofilm matrix. Nature Reviews Microbiology, 8, 623–633. https://www.nature.com/articles/nrmicro2415

Flemming, H.-C., Wingender, J., Mayer, C., Korstgens, V., and Borchard, W., 2000. Cohesiveness in biofilm matrix polymers, in Allison, D. and Gilbert P. (Eds.), Symposium of the Society for General Microbiology 59, Cambridge: Cambridge University Press, pp. 87–105.

George H.F. and Qureshi F., 2013. Newton's law of viscosity, newtonian and non-newtonian fluids, in: Wang Q.J., Chung YW. (Eds.), Encyclopedia of Tribology. Springer, Boston, MA. https://doi.org/10.1007/978-0-387-92897-5_143.

Gerbersdorf, S.U. and Wieprecht, S., 2014. Biostabilization of cohesive sediments: Revisiting the role of abiotic conditions, physiology and diversity of microbes, polymeric secretion, and biofilm architecture. Geobiology, 13, 68–97. https://doi.org/10.1111/gbi.12115

Haughton, P., Davis, C., McCaffrey, W. and Barker, S., 2009. Hybrid sediment gravity flow deposits – Classification, origin and significance. Marine and Petroleum Geology, 26, 1900–1918. https://doi.org/10.1016/j.marpetgeo.2009.02.012

Heerema, C.J., Talling, P.J., Cartigny, M.J., Paull, C.K., Bailey, L., Simmons, S.M., Parsons, D.R., Clare, M.A., Gwiazda, R., Lundsten, E., Anderson, K., Maier, K.L., Xu, J.P., Sumner, E.J., Rosenberger, K., Gales, J., McGann, M., Carter, L. and Pope, E., 2020. What determines the downstream evolution of turbidity currents? Earth and Planetary Science Letters, 532, 116023. https://doi.org/10.1016/j.epsl.2019.116023

Hermidas, N., Eggenhuisen, J.T., Jacinto, R.S., Luthi, S.M., Toth, F. and Pohl, F., 2018. A classification of clay-rich subaqueous density flow structures. Journal of Geophysical Research: Earth Surface, 123, 945–966. https://doi.org/10.1002/2017JF004386

Hope, J., Malarkey, J., Baas, J., Peakall, J., Parsons, D., Manning, A., Bass, S., Lichtman, I., Thorne, P., Ye, L. and Paterson, D., 2020. Interactions between sediment microbial ecology and physical dynamics drive heterogeneity in contextually similar depositional systems. Limnology & Oceanography, 65, 2403–2419. https://doi.org/10.1002/lno.11461

Inman, D.L., Nordstrom, C.E. and Flick, R.E., 1976. Currents in submarine canyons: An air–sea–land interaction. Annual Review of Fluid Mechanics, 8, 275–310. https://doi.org/10.1146/annurev.fl.08.010176.001423

Iverson, R.M., 1997. The physics of debris flows. Reviews of Geophysics, 35, 245–296. https://doi.org/10.1029/97RG00426

Johnson, H.P., Gomberg, J.S., Hautala, S.L. and Salmi, M.S., 2017. Sediment gravity flows triggered by remotely generated earthquake waves. Journal of Geophysical Research: Solid Earth, 122, 4584–4600. https://doi.org/10.1002/2016JB013689

Kneller, B. and Buckee, C., 2000. The structure and fluid mechanics of turbidity currents: A review of some recent studies and their geological implications. Sedimentology, 47, 62–94.

Kuenen, P.H., 1951. Properties of turbidity currents of high density. Society of Economic Palaeontologists and Mineralogists, Special Publication, 2, 14–33. https://archives.datapages.com/data/sepm_sp/SP2/Properties_of_Turbidity.htm

Kuenen, P.H., 1965. Experiments in connection with turbidity currents and clay-suspensions. 7th Symposium of the Colston Research Society, Volume XVII: University of Bristol, Butterworths Scientific Publications, London, pp. 48–71.

Lowe, D.R., 1979. Sediment gravity flows: Their classification and some problems of application to natural flows and deposits. SEPM, Special Publication 27, 75–82. https://pages.uoregon.edu/rdorsey/SedFlows/Lowe1979.pdf

Lowe, D.R., 1982. Sediment gravity flows: II Depositional models with special reference to the deposits of high-density turbidity currents. Journal of Sedimentary Research, 52, 279–297. https://doi.org/10.1306/212F7F31-2B24-11D7-8648000102C1865D

Malarkey, J., Baas, J.H., Hope, J.A., Aspden, R.J., Parsons, D.R., Peakall, J., Paterson, D.M., Schindler, R.J., Ye, L., Lichtman, I.D., Bass, S.J., Davies, A.G., Manning, A.J. and Thorne, P.D., 2015. The pervasive role of biological cohesion in bedform development. Nature Communications, 6, 6257. https://doi.org/10.1038/ncomms7257

Manica, R., 2012. Sediment Gravity Flows: Study Based on Experimental Simulations, in: Schulz, H., Lobosco, R. and Simoes, A. (Eds.), Hydrodynamics – Natural Water Bodies, IntechOpen, London, pp. 263–286.

Mehta, A.J., 2013. An Introduction to Hydraulics of Fine Sediment Transport. Advanced Series on Ocean Engineering: Volume 38: University of Florida, USA, 1060 pp.

Middleton, G.V., 1993. Sediment deposition from turbidity currents. Annual Review of Earth and Planetary Sciences, 21, 89–114. https://doi.org/10.1146/annurev.ea.21.050193.000513

Middleton, G.V., and Hampton, M.A., 1973. Sediment gravity flows: Mechanics of flow and deposition, in Middleton, G.V., and Bouma, A.H., (Eds.), Turbidites and Deep Water Sedimentation : SEPM, Pacific Coast Section, Short Course, Anaheim, California, 1–38.

Middleton, G.V. and Neal, W.J., 1989. Experiments on the thickness of beds deposited by turbidity currents. Journal of Sedimentary Research, 59, 297–307. https://doi.org/10.1306/212F8F7B-2B24-11D7-8648000102C1865D

Middleton, G.V. and Southard, J.B., 1984. Mechanics of Sediment Movement. SEPM Society for Sedimentary Geology, 3, 401 pp. http://dx.doi.org/10.2110/scn.84.03

Mohrig, D., Ellis, C., Parker, G., Whipple, K.X. and Hondzo, M., 1998. Hydroplaning of subaqueous debris flows. GSA Bulletin, 110, 387–394. https://doi.org/10.1130/0016-7606(1998)110<0387:HOSDF>2.3.CO;2

Mohrig, D., Elverhøi, A. and Parker, G., 1999. Experiments on the relative mobility of muddy subaqueous and subaerial debris flows, and their capacity to remobilize antecedent deposits. Marine Geology, 154, 117–129. https://doi.org/10.1016/S0025-3227(98)00107-8

Mohrig, D. and Marr, J.G., 2003. Constraining the efficiency of turbidity current generation from submarine debris flows and slides using laboratory experiments. Marine and Petroleum Geology, 20, 883–899. https://doi.org/10.1016/j.marpetgeo.2003.03.002

Mulder, T. and Alexander, J., 2001. The physical character of subaqueous sedimentary density flows and their deposits. Sedimentology, 48, 269–299. https://doi.org/10.1046/j.1365-3091.2001.00360.x

Parker, G., Garcia, M., Fukushima, Y. and Yu, W., 1987. Experiments on turbidity currents over an erodible bed. Journal of Hydraulic Research, 25, 123–147. https://doi.org/10.1080/00221688709499292

Postma, G., 1986. Classification for sediment gravity-flow deposits based on flow conditions during sedimentation. Geology, 14, 291–294. https://doi.org/10.1130/0091-7613(1986)14<291:CFSGDB>2.0.CO;2

Postma, G., 2011. Sediment gravity flow (SG), in: Singh V.P., Singh P. and Haritashya U.K. (Eds.), Encyclopedia of Snow, Ice and Glaciers. Encyclopedia of Earth Sciences Series. Springer, Dordrecht, 1005-1010.

Reading, H.G. and Richards, M., 1994. Turbidite systems in deep-water basin margins classified by grain size and feeder system. AAPG Bulletin, 78, 792–822.

Richardson, J.F. and Zaki, W.N., 1954. Sedimentation and fluidisation, part I. Transactions of the Institute of Chemical Engineering, 32, 35–53.

Sandhya, V. and Ali, S. Z., 2015. The production of exopolysaccharide by Pseudomonas putida GAP-P45 under various abiotic stress conditions and its role in soil aggregation. Microbiology, 84, 512–519. https://link.springer.com/article/10.1134/S0026261715040153

Sumner, E. J., Talling, P. J. and Amy, L. A., 2009. Deposits of flows transitional between turbidity current and debris flow. Geology, 37, 991–994. https://doi.org/10.1130/G30059A.1

Talling, P.J., 2013. Hybrid submarine flows comprising turbidity current and cohesive debris flow: Deposits, theoretical and experimental analyses, and generalized models. Geosphere, 9, 460–488. https://doi.org/10.1130/GES00793.1

Talling, P.J., Allin, J., Armitage, D.A., Arnott, R.W.C., Cartigny, M.J.B., Clare, M.A., Felletti, F., Covault, J.A., Girardclos, S., Hansen, E., Hill, P.R., Hiscott, R.N., Hogg, A.J., Clarke, J.H., Jobe, Z.R., Malgesini, G., Mozzato, A., Naruse, H., Parkinson, S. and Peel, F.J., 2015. Key future directions for research on turbidity currents and their deposits. Journal of Sedimentary Research, 85, 153–169. http://dx.doi.org/10.2110/jsr.2015.03

Talling, P.J., Paull, C.K. and Piper, D.J.W., 2013. How are subaqueous sediment density flows triggered, what is their internal structure and how does it evolve? Direct observations from monitoring of active flows. Earth-Science Reviews, 125, 244–287. https://doi.org/10.1016/j.earscirev.2013.07.005

Wan, Z., 1982. Bed material movement in hyperconcentrated flow: Technical University of Denmark, Institute of Hydrodynamics and Hydraulic Engineering, Lyngby, Series Paper 31, 79 pp.

Wang, X., Sharp, C.E., Jones, G.M., Grasby, S.E., Brady, A.L. and Dunfield, P.F., 2015. Stable-isotope probing identifies uncultured planctomycetes as primary degraders of a complex heteropolysaccharide in soil. Applied and Environmental Microbiology. 81, 4607–4615. https://doi.org/10.1128/AEM.00055-15

Widyatmoko, I., 2016. 14 - Sustainability of bituminous materials, in Khatib, J.M. (Eds.), Sustainability of Construction Materials (Second Edition). Woodhead Publishing Series in Civil and Structural Engineering, 343–370.

Wingender, J., Neu, T.R., and Flemming, H.-C., 1999. What are bacterial extracellular polymeric substances?, in Wingender, J., Neu, T.R., and Flemming, H.C. (Eds.), Microbial Extracellular Polymeric Substances: Characterization, Structure and Function, Berlin: Springer, 1–19.

Wolfaardt, G.M., Lawrence, J.R., and Korber, D R., 1999. Function of EPS, in Wingender, J., Neu, T.R., and Flemming, H.C. (Eds.), Microbial Extracellular Polymeric Substances, Berlin: Springer, 171–200.

Yong, R.N., Nakano, M., and Pusch, R., 2012. Environmental Soil Properties and Behavior: London, 1133 CRC Press, 455 pp.

Zabala, M., Cartigny, M.J.B., Talling, P.J., Parsons, D.R., Sumner, E.J., Clare, M.A., Simmons, S.M., Cooper, C. and Pope, E.L., 2017. Newly recognized turbidity current structure can explain prolonged flushing of submarine canyons. Science Advances, 3(10), e1700200. https://www.science.org/doi/10.1126/sciadv.1700200

Figure captions

Table 1. Summary of experimental data. LDTC = low-density turbidity current; HDTC = high-density turbidity current, LDTC>HDTC = low-density changing to high-density turbidity current near location of run-out.

Fig. 1. Top: Lock exchange tank. Bottom: Schematic diagram of the laboratory set up from the side. HD = high-definition.

Fig. 2. Procedure used to calculate the mean pre-deceleration head velocity. The red curve delimits the 23% and 64% locations along the flow path, on which the mean pre-deceleration head velocity calculations are based, where 0% is the gate location and 100% is the run-out distance of the flow or the end of the tank for flows that reflected off the end wall.

Fig. 3. Particle settling velocity against EPS concentration for the kaolin clay, coarse silt and fine sand used in the lock-exchange experiments.

Fig. 4. Typical examples of the experimental sediment gravity flows. A) Head of low-density turbidity current Si-0, characterised by pervasive turbulence, a pointed flow front, and lack of hydroplaning (arrow). B) Head of high-density turbidity current Cl-0.15, characterised by pronounced hydroplaning at the base (arrow) and a dense, turbulence-attenuated layer overlain by a more dilute, turbulent layer; note the distinct density interface (dashed line). C, D) examples of coherent fluid entrainment structures (arrows) in flows Si-0.15 and Si-0.3, respectively. E, F) examples of bypassing flow in high-density turbidity currents Cl-0.15 and Si-0.3. G, H) Slide Cl-0.3 after moving for 0.12 m and 0.74 m in the tank, respectively. Note the lack of hydroplaning, the viscous flow character, and the minor mixing with the ambient fluid. Flow is from left to right in all pictures. Scale at bottom of images is in centimetres.

Fig. 5. Flow-type phase diagram for different EPS concentrations and sediment types. LDTC = low-density turbidity current; HDTC = high-density turbidity current, LDTC>HDTC = low-density changing

to high-density turbidity current near location of run-out; MF/DF = mud or debris flow. Dashed lines denote estimated boundaries between flow types for the clay flows. The question mark refers to a mud and debris flow phase that was observed in previous work (e.g. Baker et al., 2017; Craig et al., 2020), but that was not captured within the limited resolution of EPS concentrations in the present experiments. Note that 18.5%, 26%, and 28% clay, instead of EPS, would have to be added to the clay flows to cross the boundaries between LDTC, HDTC, MF, and slide, respectively (Baker et al., 2017). These clay concentrations are two orders of magnitude higher than the boundary EPS concentrations, demonstrating the strong cohesive properties of EPS.

Fig. 6. Head velocity against distance along tank for all flows laden with (A) kaolin clay, (B) coarse silt, and (C) fine sand, with and without EPS. The head velocities of the bypassing part of flows are given in orange.

Fig. 7. Mean pre-deceleration head velocity and standard deviation of the mean (vertical lines) against EPS concentration for kaolin clay, coarse silt, and fine sand. LDTC = low-density turbidity current; HDTC = high-density turbidity current.

Fig. 8. Run-out distance against EPS concentration for kaolin clay, coarse silt and fine sand flows. Dashed blue line and green data point at 0% EPS denote minimum run-out distances, limited by the 4.6-m length of the lock-exchange tank. Note that the plotted run-out distances exclude the bypassing part of the flows.

Fig. 9. Deposit thickness trends for all flows that did not reflect off the end of the lock-exchange tank. A) Kaolin clay and coarse silt deposits. B) Fine sand deposits.

Fig. 10. Conceptual model summarising the effect of key parameters on flow mobility (top) and the dependence of type and run-out distance of sediment gravity flows on these parameters, informed by the laboratory experiments (bottom). The column labelled 'Dominant process' provides the dominant physical or biological controls on run-out distance.

Fig. 11. Deposit steepness against EPS concentration for all flows that did not reflect off the end of the lock-exchange tank.

Figure 1

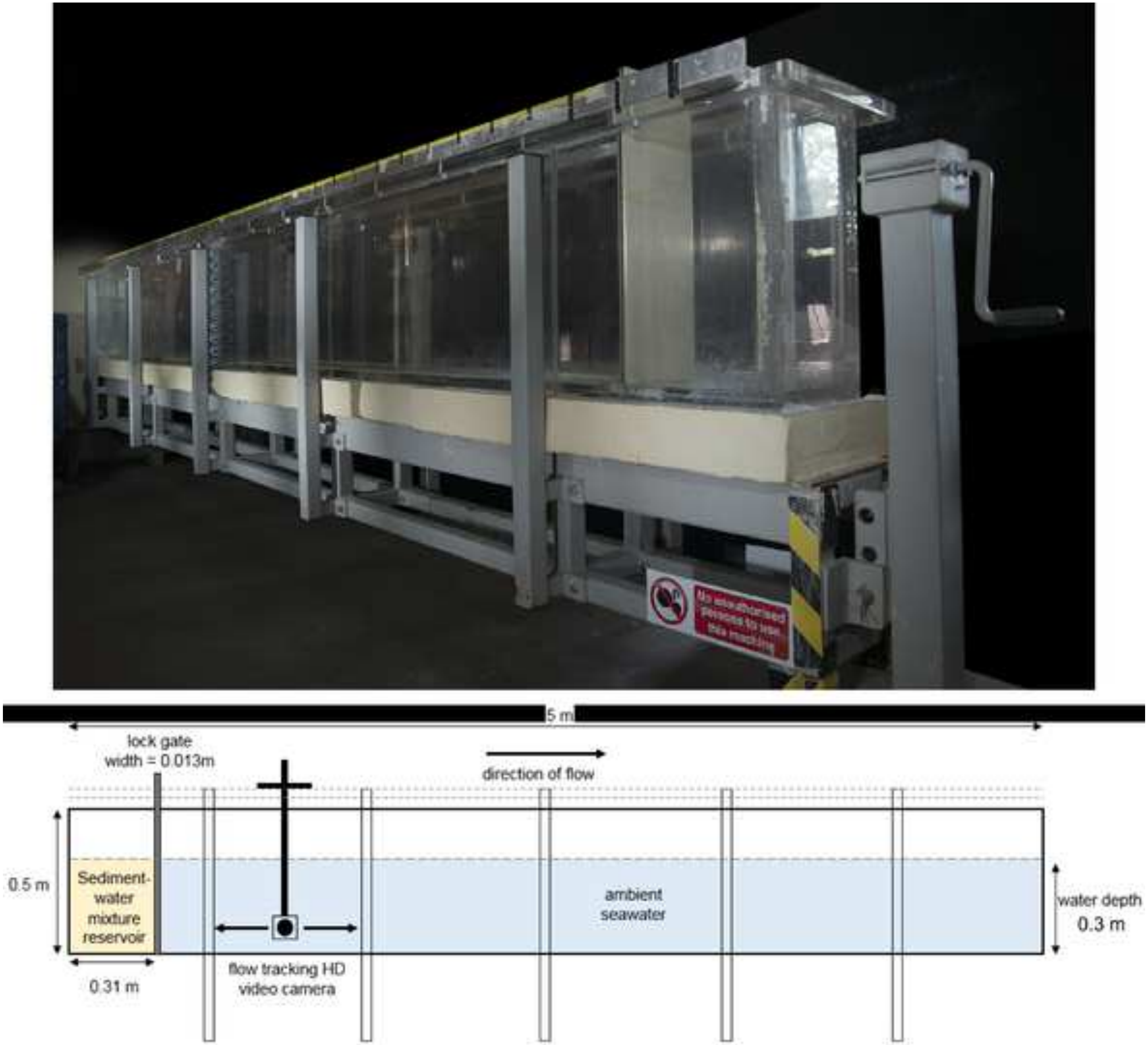
5 m
lock gate
width = 0.013m
direction of flow
0.5 m
Sediment-
water
mixture
reservoir
0.31 m
flow tracking HD
video camera
ambient
seawater
water depth
0.3 m

Figure 2

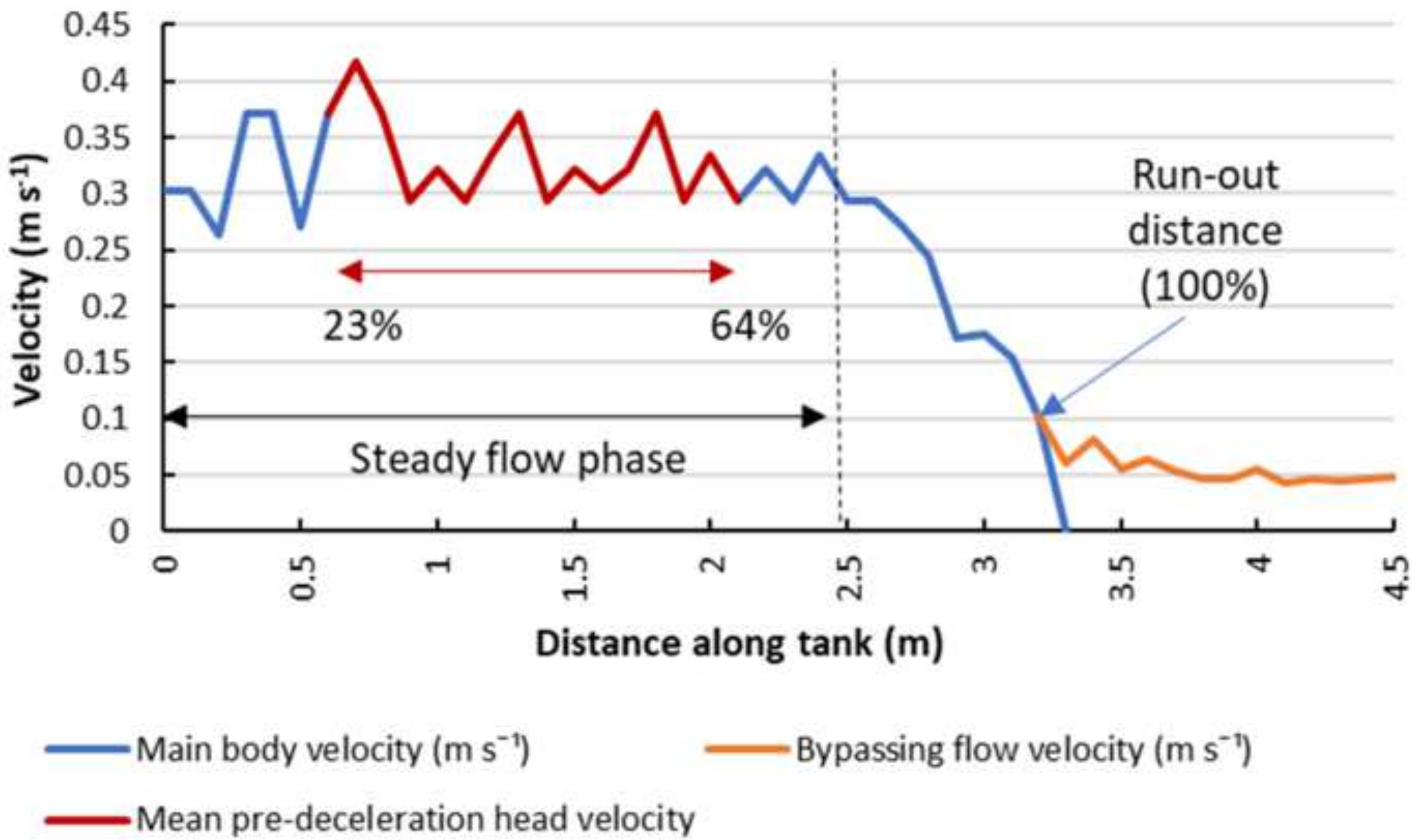
0.45
0.4
0.35
0.3
0.25
0.2
0.15
0.1
0.05
0
Velocity (m s-1)
0
0.5
1
1.5
2
2.5
3
3.5
4
4.5
Distance along tank (m)
23%
64%
Steady flow phase
Run-out distance (100%)
Main body velocity (m s-1)
Bypassing flow velocity (m s-1)
Mean pre-deceleration head velocity

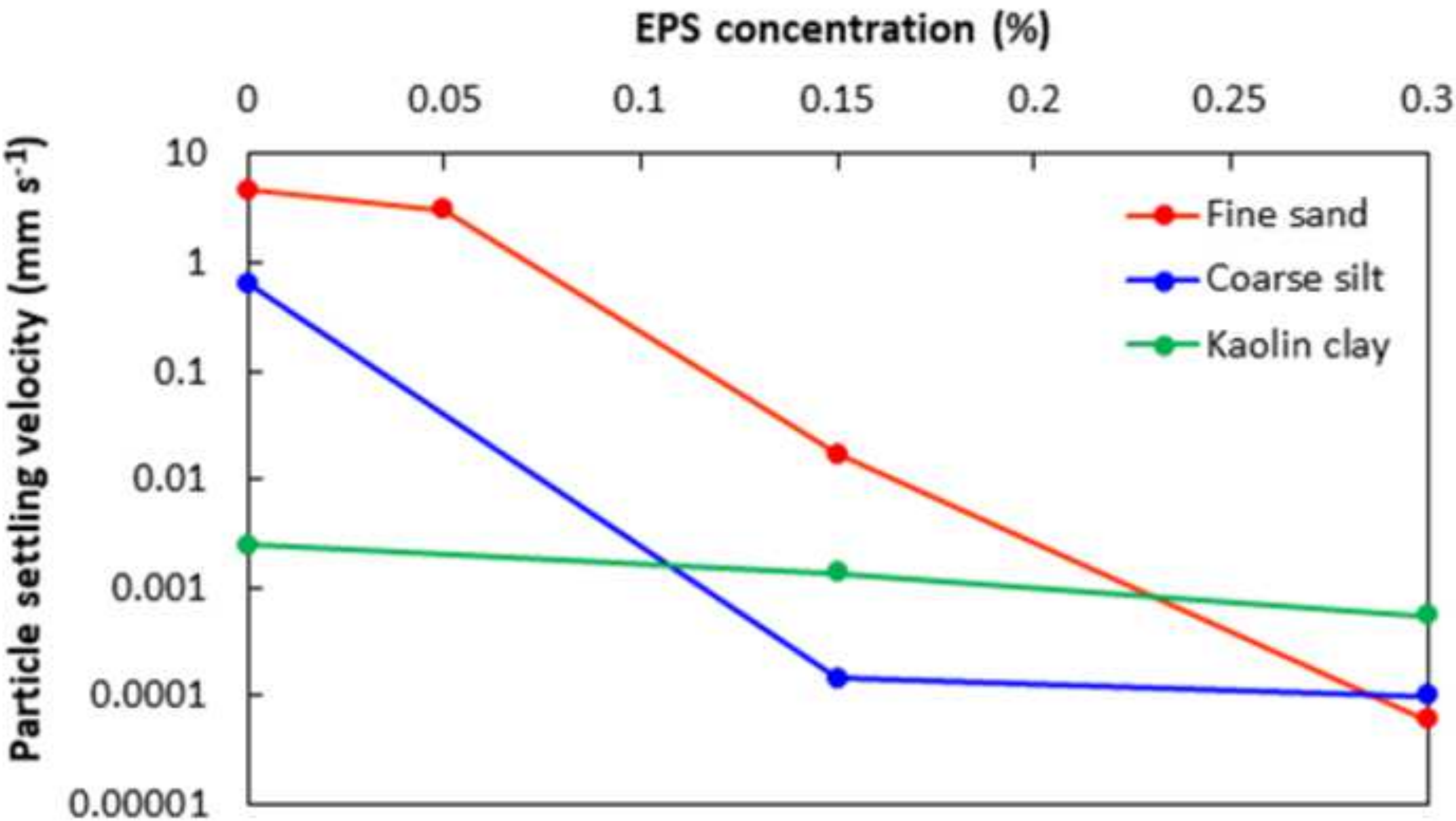
EPS concentration (%)
0
0.05
0.1
0.15
0.2
0.25
0.3
Particle settling velocity (mm s-1)
10
1
0.1
0.01
0.001
0.0001
0.00001
Fine sand
Coarse silt
Kaolin clay

Figure 4

Click here to access/download;Figure;Sobocinska & Baas, Fig. 4.tif

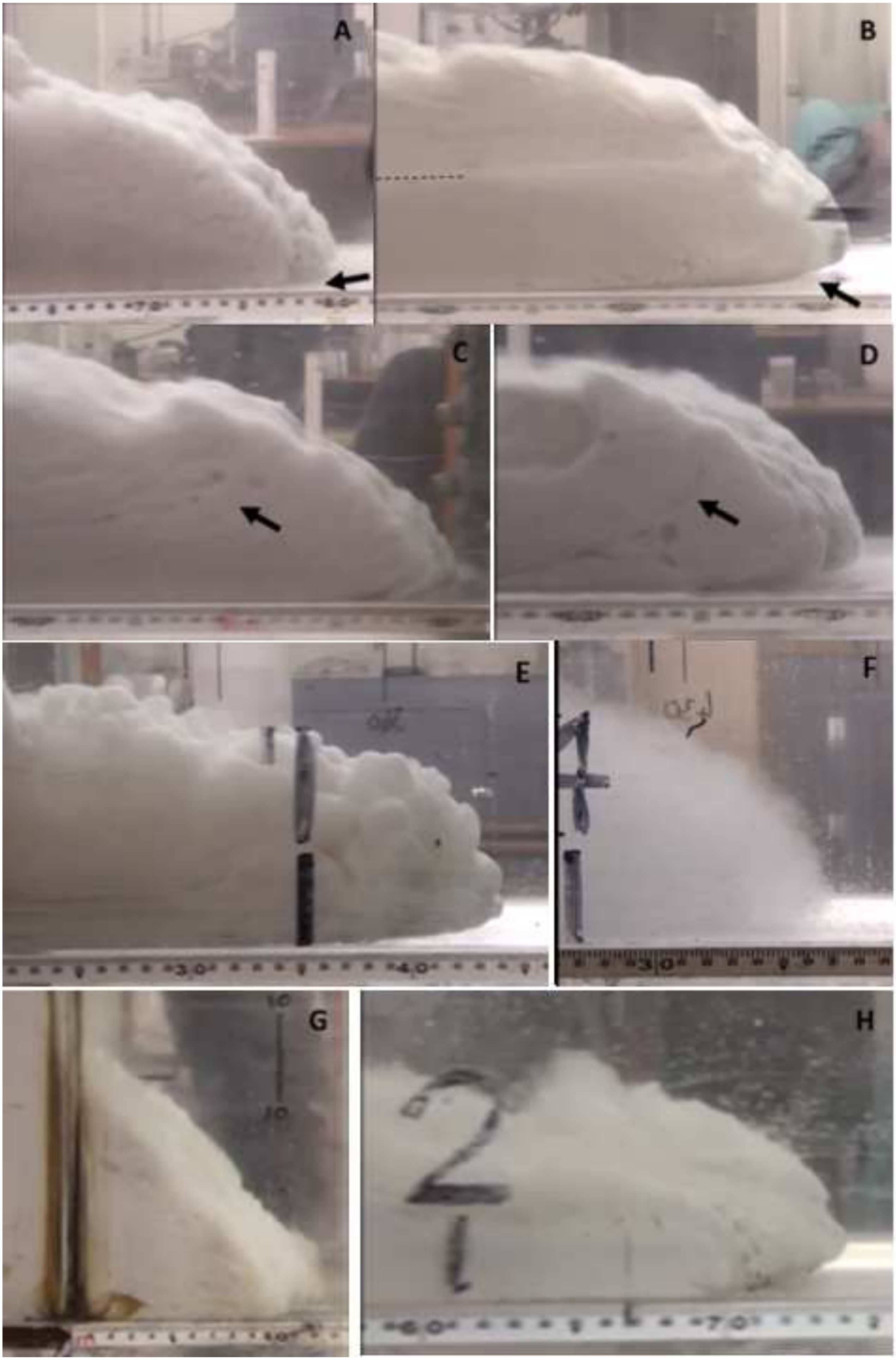

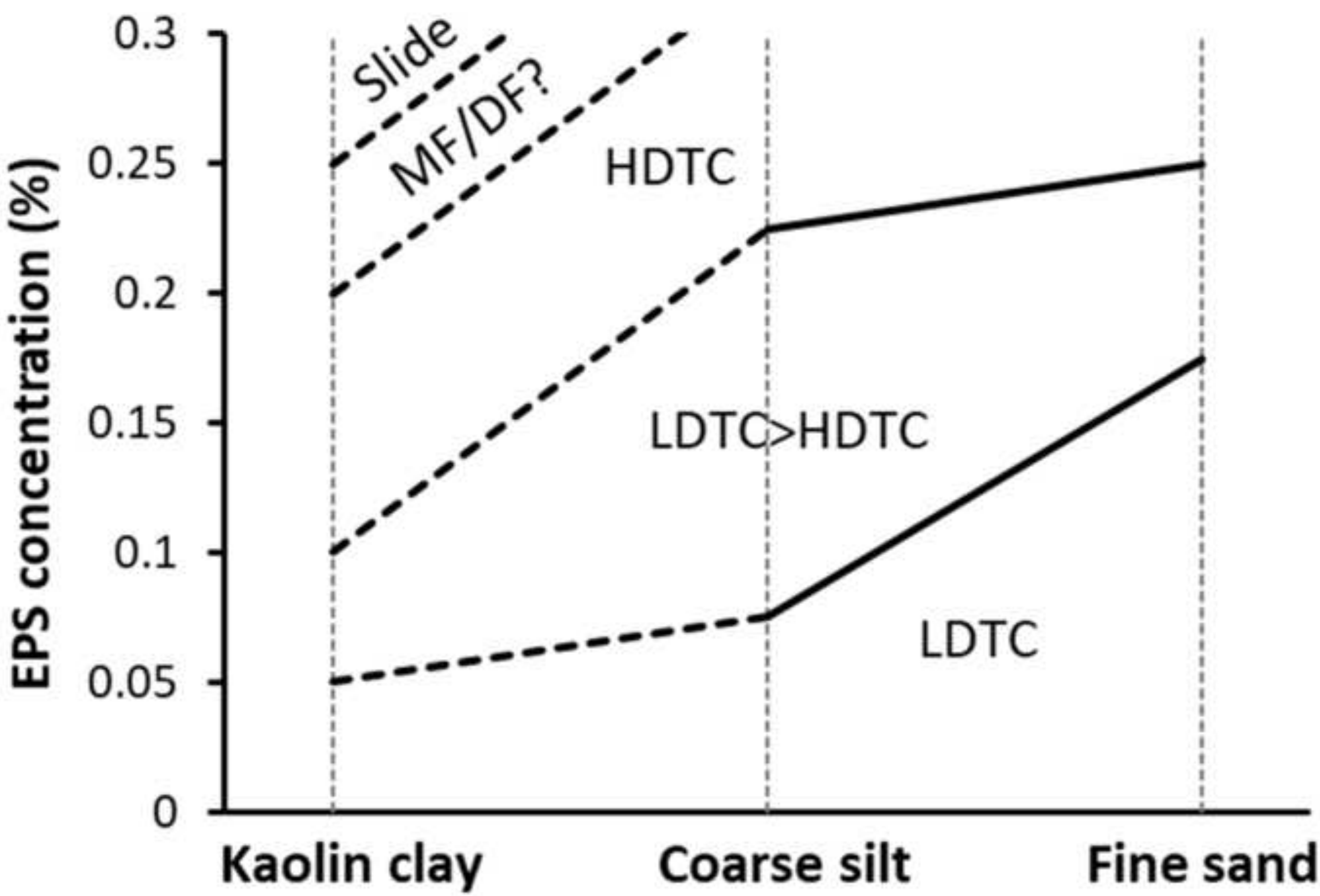

0.3
0.25
0.2
0.15
0.1
0.05
0
EPS concentration (%)
Slide
MF/DF?
HDTC
LDTC>HDTC
LDTC
Kaolin clay
Coarse silt
Fine sand

Figure 6

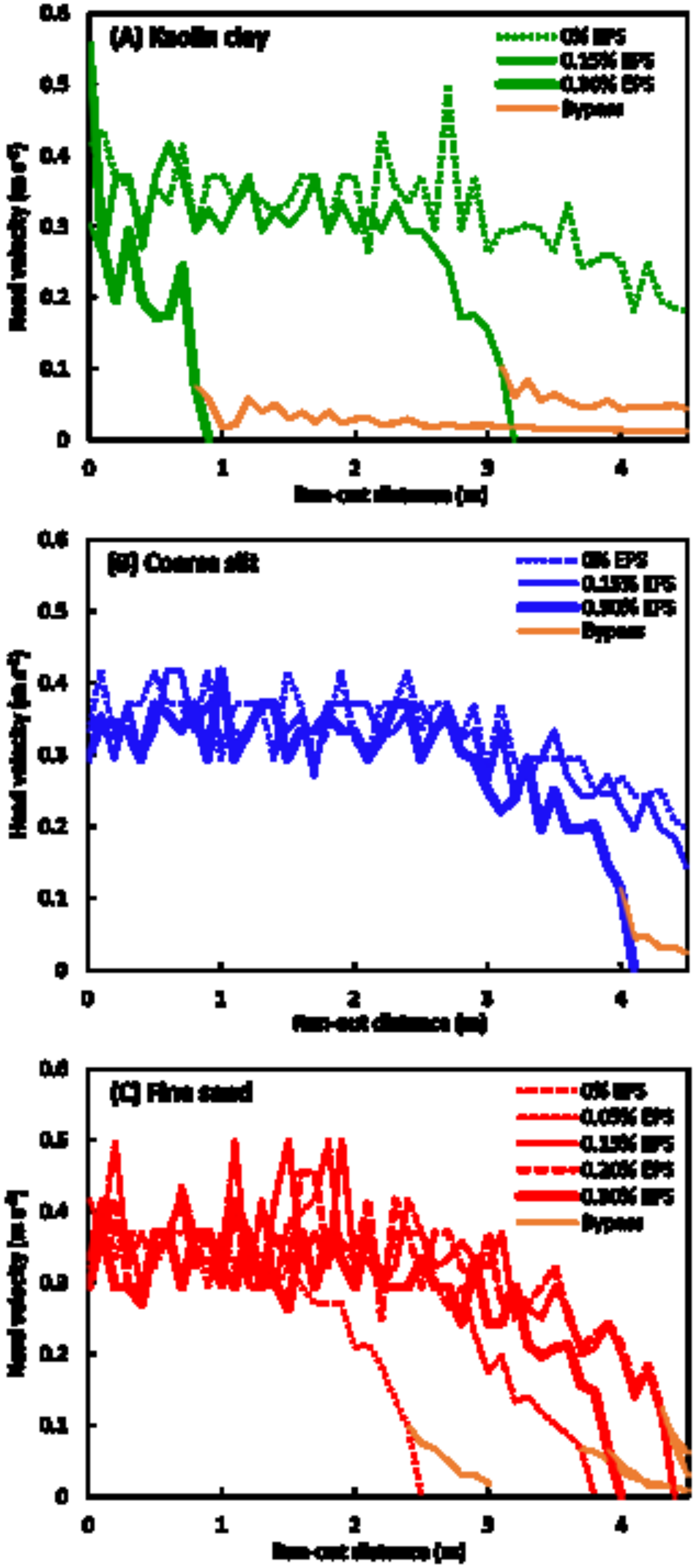
(A) Kaolin clay
0% EPS
0.15% EPS
0.30% EPS
Bypass
(B) Coarse silt
(C) Fine sand
0.05% EPS
0.20% EPS
Head velocity (m s-1)
Run-out distance (m)

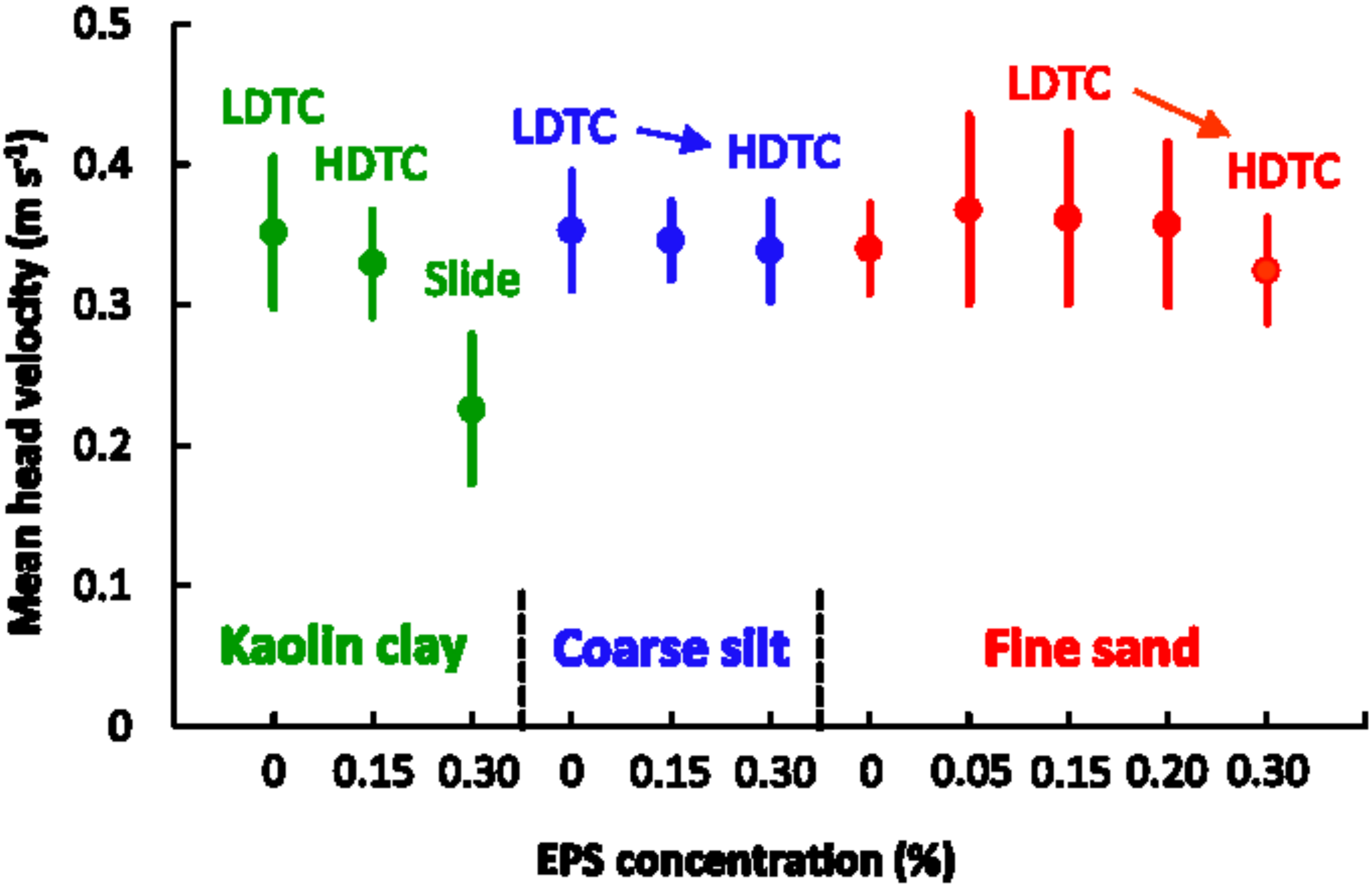
0.5
0.4
0.3
0.2
0.1
0
Mean head velocity (m s-1)
LDTC
HDTC
Slide
LDTC
HDTC
LDTC
HDTC
Kaolin clay
Coarse silt
Fine sand
0
0.15
0.30
0
0.15
0.30
0
0.05
0.15
0.20
0.30
EPS concentration (%)

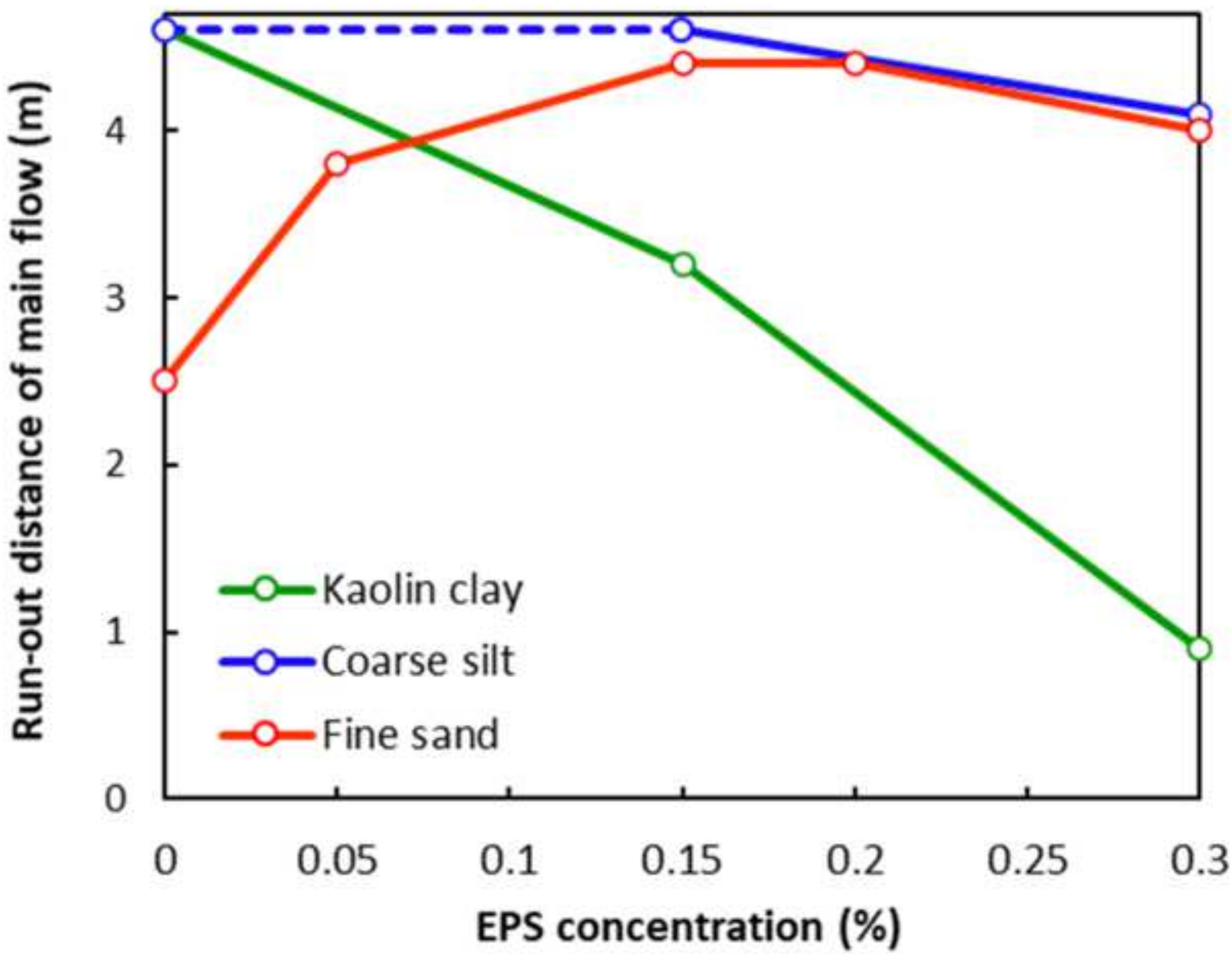
Run-out distance of main flow (m)
0
1
2
3
4
0
0.05
0.1
0.15
0.2
0.25
0.3
EPS concentration (%)
Kaolin clay
Coarse silt
Fine sand

Figure 9

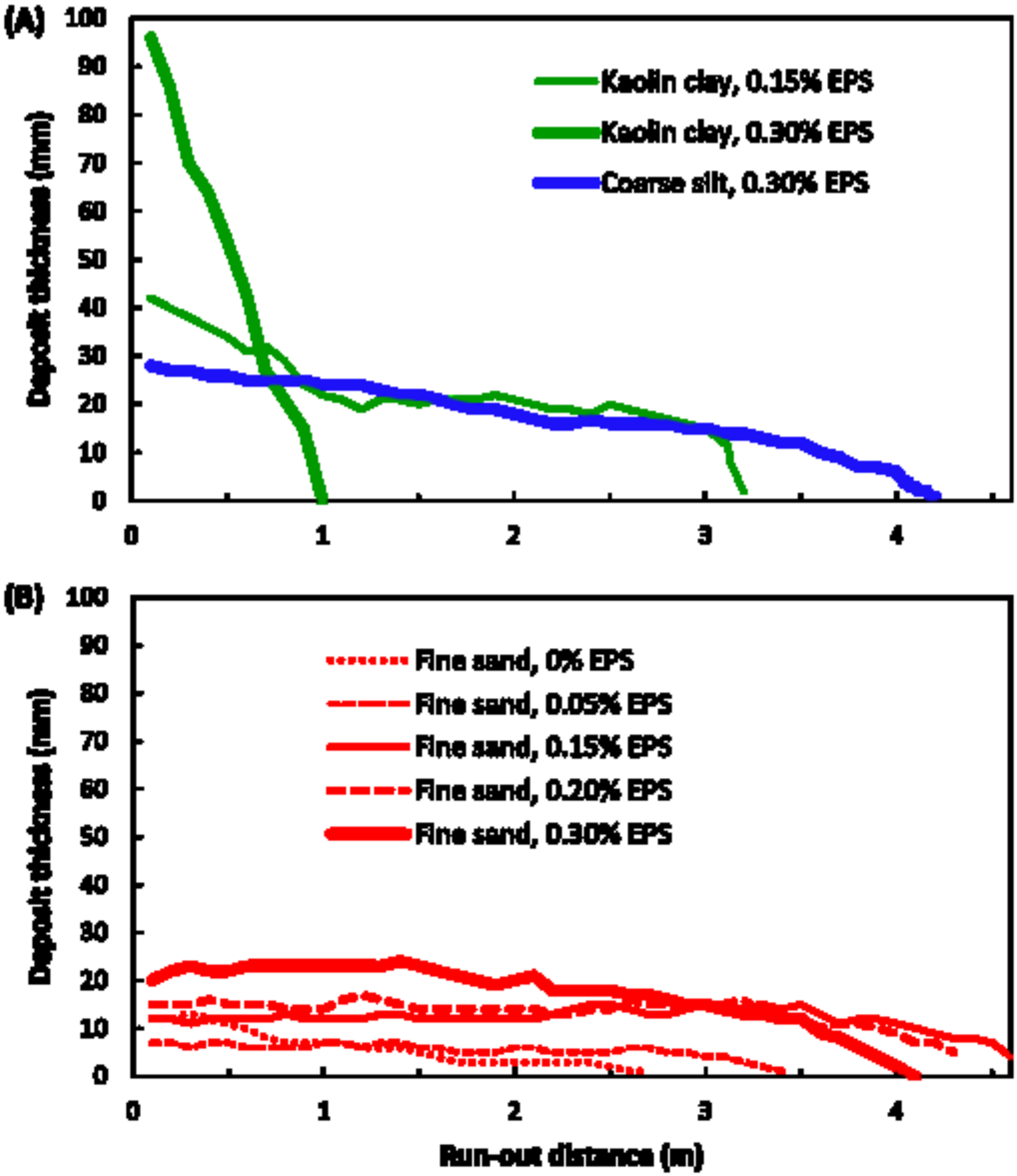
(A)
Kaolin clay, 0.15% EPS
Kaolin clay, 0.30% EPS
Coarse silt, 0.30% EPS
Deposit thickness (mm)
100
90
80
70
60
50
40
30
20
10
0
0
1
2
3
4
(B)
Fine sand, 0% EPS
Fine sand, 0.05% EPS
Fine sand, 0.15% EPS
Fine sand, 0.20% EPS
Fine sand, 0.30% EPS
Deposit thickness (mm)
Run-out distance (m)

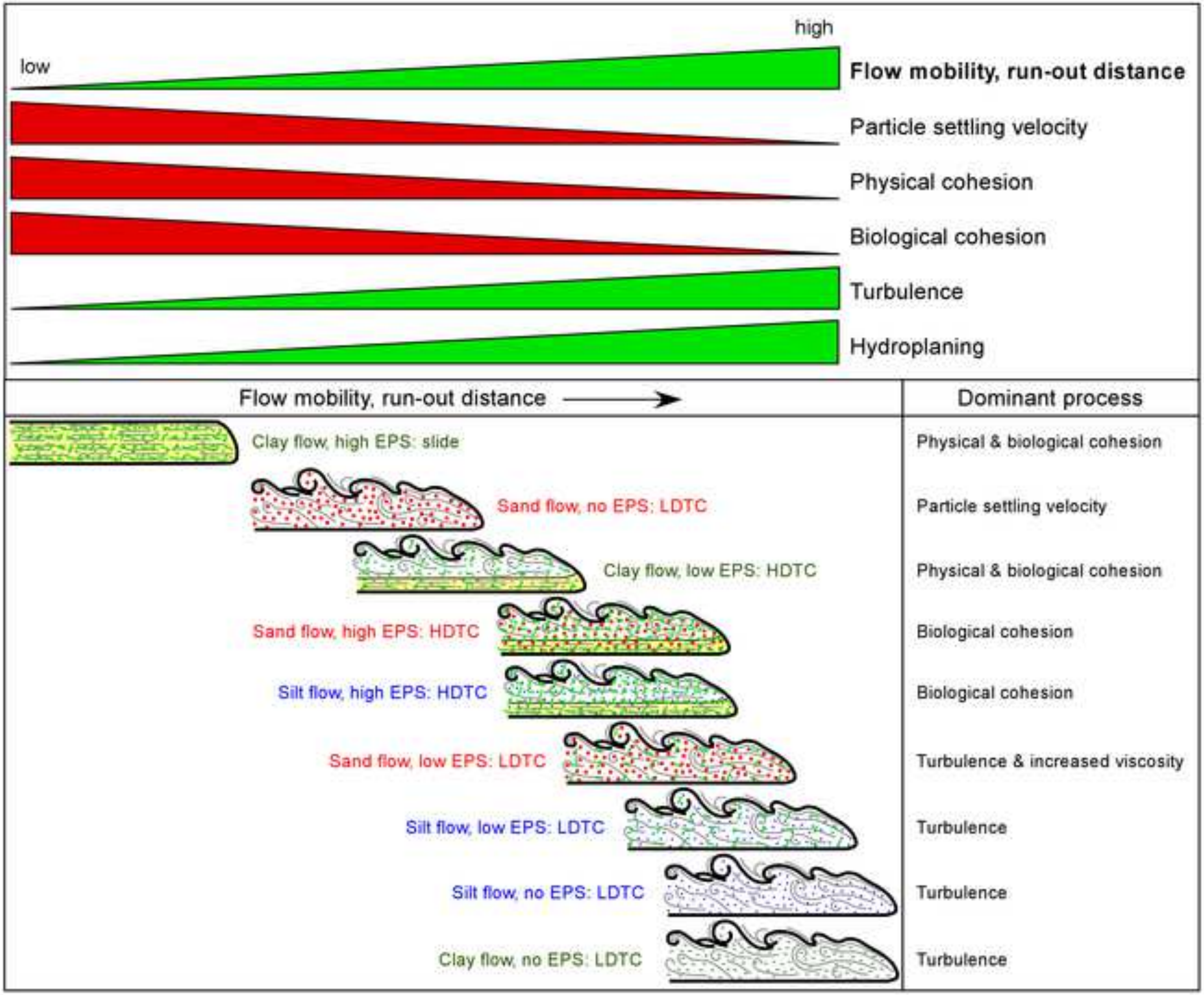

low
high
Flow mobility, run-out distance
Particle settling velocity
Physical cohesion
Biological cohesion
Turbulence
Hydroplaning
Flow mobility, run-out distance
Dominant process
Clay flow, high EPS: slide
Physical & biological cohesion
Sand flow, no EPS: LDTC
Particle settling velocity
Clay flow, low EPS: HDTC
Physical & biological cohesion
Sand flow, high EPS: HDTC
Biological cohesion
Silt flow, high EPS: HDTC
Biological cohesion
Sand flow, low EPS: LDTC
Turbulence & increased viscosity
Silt flow, low EPS: LDTC
Turbulence
Silt flow, no EPS: LDTC
Turbulence
Clay flow, no EPS: LDTC
Turbulence

Figure 11

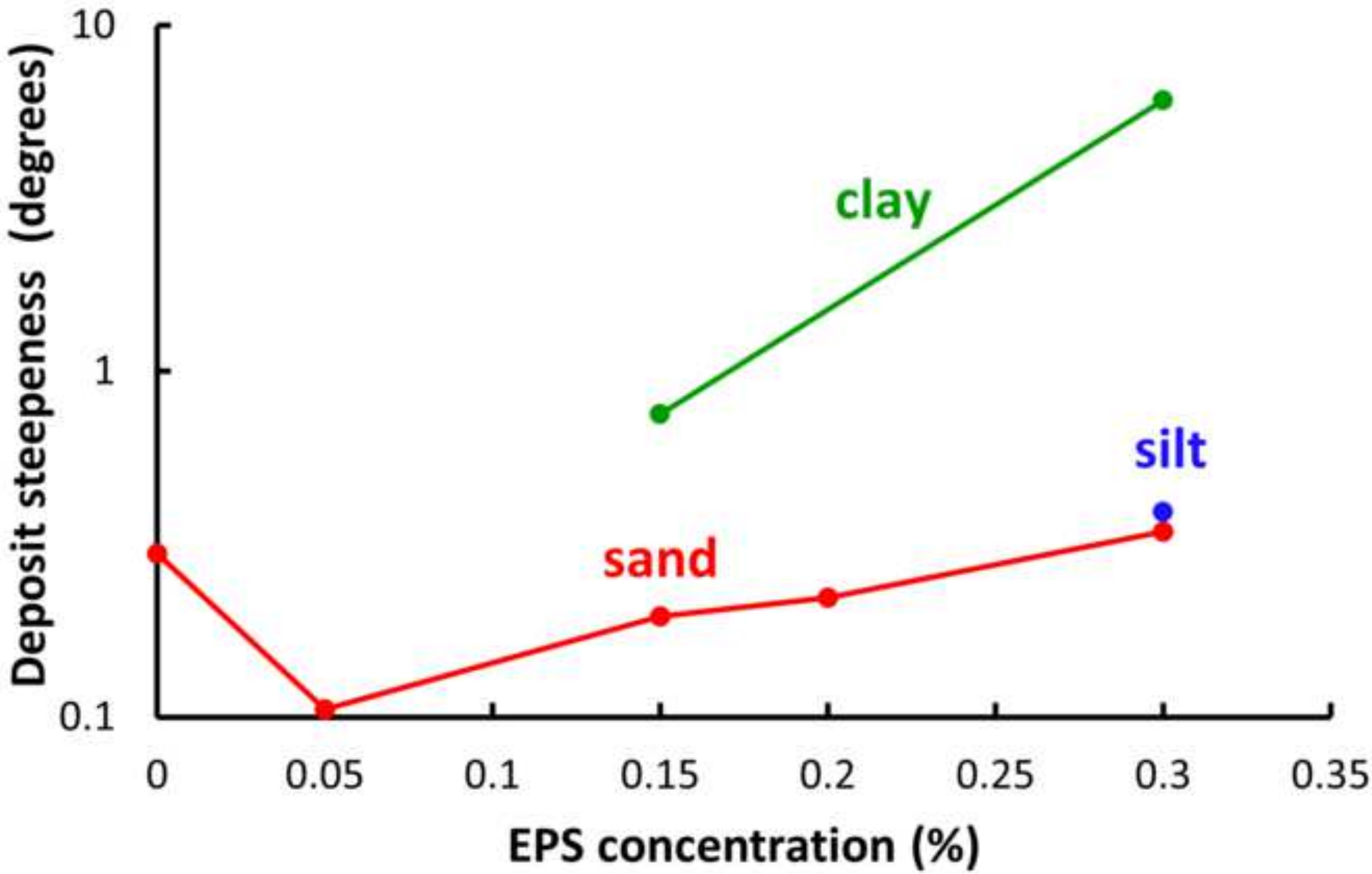
Deposit steepeness (degrees)
10
1
0.1
clay
silt
sand
0
0.05
0.1
0.15
0.2
0.25
0.3
0.35
EPS concentration (%)

Table 1. Summary of experimental data. LDTC = low-density turbidity current; HDTC = high-density turbidity current, LDTC>HDTC = low-density changing to high-density turbidity current near location of run-out.

Experimental run	Sediment type	EPS concentration (%)	Pre-deceleration velocity (m s^{-1})	Froude number*	Run-out distance (m)	Flow type
Cl-0	Clay	0	0.351	0.66	> 4.6**	LDTC
Cl-0.15	Clay	0.15	0.329	0.62	3.2	HDTC
Cl-0.3	Clay	0.3	0.226	0.82	0.9	Slide
Si-0	Coarse silt	0	0.353	0.70	> 4.6**	LDTC
Si-0.15	Coarse silt	0.15	0.346	0.65	> 4.6**	LDTC> HDTC
Si-0.3	Coarse silt	0.3	0.338	0.64	4.1	HDTC
Sa-0	Fine sand	0	0.340	0.75	2.5 (2.6)***	LDTC
Sa-0.05	Fine sand	0.05	0.368	0.71	3.8	LDTC
Sa-0.15	Fine sand	0.15	0.362	0.71	4.4 (4.6)***	LDTC
Sa-0.2	Fine sand	0.2	0.357	0.74	4.4	LDTC> HDTC
Sa-0.3	Fine sand	0.3	0.324	0.66	4 (4)***	HDTC

* Densimetric Froude number was calculated from flow thickness at x = 1.5 m (except for Cl-03: x = 0.5 m), mean pre-deceleration head velocity, and initial flow density.

** Flow reached the end of lock-exchange tank.

*** Run-out distances between brackets are based on replicate experiments.

Declaration of interests

☒The authors declare that they have no known competing financial interests or personal relationships that could have appeared to influence the work reported in this paper.

☐The authors declare the following financial interests/personal relationships which may be considered as potential competing interests: